

Observation of tearing mode deceleration and locking due to eddy currents induced in a conducting shell

B. E. Chapman

Department of Physics, University of Wisconsin-Madison, Madison, Wisconsin 53706

R. Fitzpatrick

Institute for Fusion Studies, Department of Physics, University of Texas at Austin, Austin, Texas 78712

D. Craig

Department of Physics, University of Wisconsin-Madison, Madison, Wisconsin 53706

P. Martin

Consorzio RFX, Associazione EURATOM-ENEA sulla Fusione, Corso Stati Uniti 4, 35127 Padova, Italy and Istituto Nazionale Fisica della Materia, INFN, Padova, Italy

G. Spizzo

Consorzio RFX, Associazione EURATOM-ENEA sulla Fusione, Corso Stati Uniti 4, 35127 Padova, Italy

(Received 29 October 2003; accepted 30 January 2004; published online 16 April 2004)

Growth to large amplitude of a single core-resonant tearing mode in the Madison Symmetric Torus [R. N. Dexter *et al.*, *Fusion Technol.* **19**, 131 (1991)] reversed-field pinch is accompanied by braking and eventual cessation of mode rotation. There is also a concurrent deceleration of bulk plasma rotation. The mode deceleration is shown to be well described by a time-dependent version of a magnetohydrodynamical model [R. Fitzpatrick *et al.*, *Phys. Plasmas* **6**, 3878 (1999)] in which a braking torque originates from eddy currents induced by the rotating mode in the conducting shell surrounding the plasma. According to the model, the electromagnetic braking torque is localized to the plasma in the immediate vicinity of the mode's resonant surface, but viscosity transfers the torque to the rest of the plasma. Parametrizing the plasma viscous momentum diffusivity in terms of the global momentum confinement time, the model is used to predict both the momentum confinement time and the time evolution of the decelerating mode velocity. In both respects, the model is quite consistent with experimental data. © 2004 American Institute of Physics. [DOI: 10.1063/1.1689353]

I. INTRODUCTION

Toroidal plasma rotation is important, and in some cases critical, in toroidal magnetic fusion configurations such as the tokamak and reversed-field pinch. One reason for this is that with sufficiently fast plasma rotation, internally resonant resistive tearing modes corotate with the plasma. However, if the plasma rotation becomes too small, then such modes can lock (i.e., become stationary in the laboratory frame of reference). Mode locking has a variety of negative consequences. For example, locking in the tokamak often results in a disruption or total loss of plasma containment. In the reversed-field pinch, locking does not usually cause disruptions, but it can give rise to enhanced plasma-wall interaction and a consequent degradation of energy confinement.

In both the tokamak and reversed-field pinch (RFP), damping of plasma rotation and mode locking occur under a variety of circumstances. In both configurations, mode deceleration and locking can occur with the growth to large amplitude of a single, internally resonant tearing mode.¹⁻³ In the late 1980s, a theory was proposed for the tokamak and RFP that linked the deceleration and locking of a single mode directly to the amplitude of the mode.⁴⁻⁷ According to this theory, eddy currents induced in the conducting shell surrounding the plasma exert a braking torque on the plasma

in the immediate vicinity of the mode's resonant surface. Since the rotation of a resonant tearing mode is due to rotation of this local plasma, damping the local plasma rotation leads directly to a decrease in the mode rotation and can eventually cause locking. This initial theoretical work was later augmented for the tokamak with a more detailed model which takes into account the viscous coupling of the local plasma to the bulk plasma, described further below.⁸ The physics incorporated in this augmented model also formed the basis of a revised model for the RFP.⁹

While there are differences in detail in the tokamak and RFP models^{8,9} for braking due to eddy currents, the basic physics of the models is generic. Fundamentally, the models describe a mutual torque exerted between the plasma and conducting shell, leading to the transfer of plasma angular momentum to the shell. A rotating, internally resonant tearing mode, amplitude \mathbf{b}_{mode} , surrounded by a conducting shell induces in the shell a pattern of eddy (or image) currents with the same toroidal and poloidal mode number as the mode. The eddy currents generate a rotating magnetic perturbation, amplitude \mathbf{b}_{eddy} , whose phase lags that of the mode. This lag is due to the finite self-inductance and resistance of the shell. A sheetlike current $\mathbf{j}_{\text{sheet}} = (\nabla \times \mathbf{b}_{\text{eddy}}) / \mu_0$ is generated in the plasma in the vicinity of the tearing mode's

resonant surface. Given the phase lag between $\mathbf{j}_{\text{sheet}}$ and \mathbf{b}_{mode} , a (nonlinear) $\mathbf{j}_{\text{sheet}} \times \mathbf{b}_{\text{mode}}$ electromagnetic torque is exerted on the local plasma which always opposes the local plasma and mode rotation.

Assuming a tearing mode of sufficient amplitude, a magnetic island will be present, centered on the mode's resonant surface. There is little or no net plasma flow relative to this island; i.e., the mode corotates with the plasma in the vicinity of the mode's resonant surface. Consider the case of a growing mode and, hence, a growing braking torque. A key assumption of the model is that the local (island) plasma is viscously coupled to the bulk plasma external to the island. Thus, as the island plasma begins to decelerate, a countering viscous torque develops. If the braking torque continues to grow, substantial braking of the island plasma and island can occur, but not without substantial deceleration of the bulk plasma as well. The mode braking and locking cannot occur on a time scale significantly faster than that of global viscous diffusion. Note that as the mode rotation velocity approaches zero, the phase lag between $\mathbf{j}_{\text{sheet}}$ and \mathbf{b}_{mode} also approaches zero, resulting in a vanishingly small torque. Hence, actual locking cannot take place solely due to eddy currents. However, eddy currents can decelerate the mode to an extent that other sources of braking torque can easily lock it.

There have been relatively few published experimental tests of eddy current braking theory. Tests of the theory in its first incarnation,⁴⁻⁷ without a detailed accounting of the plasma viscous response, were made in the tokamak.¹ and RFP³ to account for the growth of a single tearing mode accompanied by deceleration and eventual locking of the mode. Qualitative consistency with the theory was reported. The theory was also used successfully in a tokamak to account for so-called forbidden bands of mode rotation frequency, where a mode transitions rapidly across a particular band of frequency when the mode is decelerating or reaccelerating.¹⁰ The modified theory for the RFP⁹ was also applied to predict a mode amplitude threshold for locking in three RFP experiments.^{9,11-13} Consistency with the theory was found, in that mode amplitudes in locked plasmas were above the predicted threshold. Most recently, an estimate of the eddy-current torque was made to try to account for two cases of varying mode rotation behavior in a tokamak.¹⁴ The plasma viscous response was not included in this calculation. Contrary to the aforementioned papers, it was concluded in this latest work that the mode rotation behavior was not significantly affected by the eddy-current torque.

In part due to the relative paucity of detailed comparisons of experiment to theory, and in light of the paper just described, the explanation of mode deceleration and locking in terms of the torque from eddy currents cannot be said to be universally accepted. There has yet to be a definitive experimental test of the more recent braking theories for the tokamak⁸ and RFP.⁹

In this paper, we report a fully quantitative, dynamical test of eddy-current braking theory. The test is conducted using RFP plasmas in the Madison Symmetric Torus (MST)¹⁵ in which growth to large amplitude of a single core-resonant tearing mode (poloidal mode number $m=1$) is ac-

companied by deceleration and locking of the mode. We test the RFP theory described in Ref. 9, but we have extended this theory to include time-dependent mode growth. Modeling the entire braking sequence, we find that the theory fits the data quite well. We have also ruled out other causes of braking and locking, such as the partially corrected magnetic error field, which play a role in some MST plasmas.^{16,17}

Concurrent with the deceleration and locking of the single tearing mode in these MST plasmas, there is also a deceleration of the bulk plasma. This mode and plasma deceleration occurs without any significant change to the global equilibrium, in terms of, e.g., the plasma current and electron density. The unchanging equilibrium, along with MST's simple, circular poloidal cross section and single, thick conducting shell, provides an ideal test bed for the theory. The deceleration occurs with different fuel isotopes, magnetic equilibria, initial mode rotation velocities, and mode growth rates, allowing tests of the model over a relatively broad parameter range and in a relatively large number of discharges. Given the assumed importance of the bulk-plasma viscous momentum diffusivity in the deceleration, we parameterize the diffusivity in terms of the global momentum confinement time (in the absence of the braking torque). The model is then used to predict both the momentum confinement time and the time evolution of the decelerating mode velocity. In both respects, the model is quite consistent with experimental data.

In Sec. II, we describe the MST device, relevant MST plasma diagnostics, and the observed mode growth and braking. We follow in Sec. III with a discussion of the causes of braking and locking in other MST plasmas, and we show that these causes do not pertain here. Section IV is devoted to a detailed discussion of the original time-independent model for braking due to eddy currents in the RFP. In Sec. V, we describe modifications to the model needed to make it time dependent and show applications of the revised model to present MST data. We summarize in Sec. VI and discuss the implications of this work for the RFP and tokamak.

II. EXPERIMENTAL APPARATUS AND BRAKING DATA

A. MST and relevant diagnostics

The data in this paper were measured in the MST RFP.¹⁵ The MST plasma is toroidal with a circular poloidal cross section. The plasma is surrounded by a single conducting shell which also serves as the vacuum vessel and single-turn toroidal field winding. The shell has a 150-cm major radius and a 52-cm minor radius (measuring out to the plasma-facing surface of the shell). The plasma minor radius is limited to about 51 cm by a distribution of tiles covering 10% of the shell surface. The shell is 5 cm thick, comprised of an aluminum alloy (6061-T6), and is largely uniform toroidally and poloidally. The primary nonuniformities are portholes, the largest of which are 11.4 cm in diameter, and two 1.3-cm-wide electrically insulated gaps (cuts). The so-called poloidal gap extends poloidally to allow poloidal flux (produced by toroidal plasma current) to enter the vessel, while

the so-called toroidal gap extends toroidally at the inboard midplane and allows toroidal flux to enter the vessel. Image currents on the surface of the conducting shell arriving at one side of the poloidal gap are able to pass to the other side by a conductor connected across the gap. No such conductor is connected across the toroidal gap. Image currents arriving at the toroidal gap pass into the toroidal magnetic field circuit, which is connected directly to the vessel.

Radial magnetic error fields occur at both gaps. In this work, we need only be concerned with error fields that have the same poloidal and toroidal mode numbers (m,n) as the single large mode, since only such resonant error fields can affect the mode's rotation.^{8,17,18} As discussed further below, this large mode has $(m,n) = (1,5)$ or $(1,6)$, depending on the magnetic equilibrium. The error field at the poloidal gap has a fairly broad m and n spectrum, including $(1,5)$ and $(1,6)$ components. However, we show below that even a relatively large resonant error field at the poloidal gap does not affect the mode's rotation. Recent measurements of the error field at the toroidal gap indicate that the resonant components are small.¹⁹ Hence, we assume here that this field plays no role.

The amplitudes and phase velocities of the internally resonant tearing modes are measured with a toroidal array of magnetic sensing coils mounted on the plasma-facing surface of the conducting shell just beyond the plasma boundary. Detection at the plasma boundary of all the core-resonant $m=1$ modes is possible given the global perturbations associated with the modes. The sensing coil array is comprised of 32 coil pairs. One coil in each pair measures the fluctuating poloidal field, while the other measures the fluctuating toroidal field. A Fourier decomposition of each set of 32 discrete signals provides the poloidal and toroidal magnetic fluctuation amplitudes of each mode, as well as each mode's toroidal phase velocity. Toroidal rotation of CV (or C^{4+}) impurity ions is measured with a passive Doppler spectrometer having a tangential-toroidal view of the plasma.²⁰ The location of the measured velocity depends on the profile of the CV emission. For the CV data shown below, the emission is strong across the plasma core, thereby allowing measurement of the CV rotation in the region where the dominant $m=1$ modes are resonant. The poloidal velocity of the modes and plasma in the core is small compared to the toroidal velocity. Hence, we consider only the toroidal component of the velocity in this paper.

B. Experimental braking data

The discharges included in this work were fueled with either hydrogen or deuterium and have toroidal plasma currents I_ϕ from 230 kA to 390 kA and a central line-averaged electron density $\langle n_e \rangle$ from $0.7 \times 10^{19} \text{ m}^{-3}$ to $1.5 \times 10^{19} \text{ m}^{-3}$. The toroidal magnetic field reversal parameter $F \equiv B_\theta(a)/\langle B_\phi \rangle$ ranges from 0 to -0.2 , where $B_\theta(a)$ is the surface toroidal magnetic field and $\langle B_\phi \rangle$ is the poloidal-cross-section average. Most of the plasmas studied here have $F=0$. The related pinch parameter $\Theta = B_\theta(a)/\langle B_\phi \rangle$, where $B_\theta(a)$ is the surface poloidal magnetic field, varies from about 1.45 to 1.70, the lower value corresponding to $F=0$ plasmas. All of the plasmas examined in this paper are re-

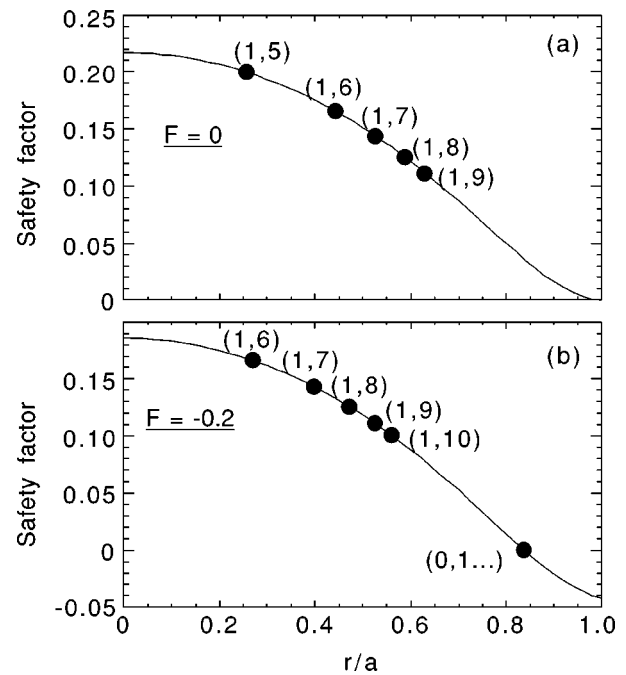


FIG. 1. Safety factor profiles reconstructed from an equilibrium model for plasmas with (a) $F=0$, $I_\phi=300$ kA, shot (1990131033) and (b) $F=-0.2$, $I_\phi=385$ kA, shot (1001112138).

ferred to as standard, since their global energy confinement time is approximately the MST standard 1 ms. We exclude from this study recently achieved plasmas in which the confinement time is substantially improved.²¹

For the $F=0$ and $F=-0.2$ plasmas studied in this paper, we show in Fig. 1 the locations and (m,n) values of the five lowest n , $m=1$ modes, resonant in the plasma core. The locations indicated are of the mode resonant surfaces. They are labeled on plots of the safety factor profile, $q(r)$, which is equal to m/n on resonant surfaces. These $m=1$ modes dominate a typical mode spectrum. One notable difference between the two q profiles in Fig. 1 is the value of $q(0)$, which determines the toroidal mode number of the innermost resonant $m=1$ mode. In the $F=0$ profile, $q(0) > 0.2$, making the $(1,5)$ mode innermost resonant. In the $F=-0.2$ profile, $q(0) < 0.2$, making the $(1,6)$ mode innermost resonant. Another notable difference between these profiles is the value of $q(a)$. With $q(a) < 0$ in the $F=-0.2$ profile, modes with $m=0$ ($n=1,2,3,\dots$) are resonant in the plasma, all at the same radius. With $q(a)=0$, the $m=0$ modes are resonant at the surface of the conducting shell. The potential significance of the $m=0$ modes in this work is discussed below.

The plasmas of interest in this paper exhibit growth to large amplitude of the innermost resonant $m=1$ mode. Mode spectra with this feature have been dubbed quasi single helicity (QSH), referring to the fact that the mode spectrum is comprised approximately of only one mode helicity (m,n) .²²⁻²⁵ A QSH spectrum appears in the $F=0$ discharge shown in Fig. 2, and it results in mode braking and locking. The evolution of the $m=1$, $n=5-9$ mode amplitudes is shown in Fig. 2(a). Until about 14 ms, the amplitudes are comparable to one another, but the $(1,5)$ mode then grows steadily and ultimately dominates the spectrum. The

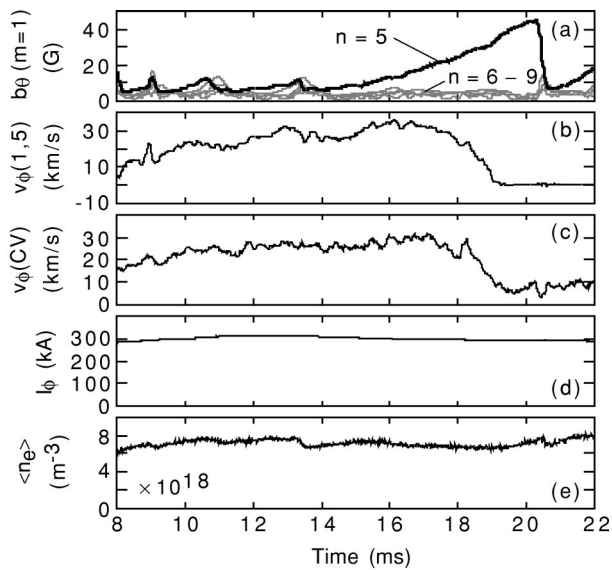


FIG. 2. From the $F=0$ plasma used in Fig. 1, (a) poloidal magnetic fluctuation amplitude of the $m=1, n=5$ mode (black line) and the $m=1, n=6-9$ modes (gray lines), (b) toroidal phase velocity of the $m=1, n=5$ mode, (c) toroidal flow velocity of CV ions, (d) toroidal plasma current, and (e) central line-averaged electron density.

roughly linear growth and eventual sudden drop of the dominant mode amplitude shown here is common to all the plasmas in this study. In other plasmas, the dominant mode amplitude grows and saturates, remaining large and constant for tens of ms, but in all cases, mode braking and locking occurs during the mode growth phase. These peaked mode spectra do not occur in all MST plasmas, even with the same operational parameters, and they appear at different times in plasmas in which they do occur.

The toroidal phase velocity of the (1,5) mode and the toroidal flow velocity of CV ions are shown in Figs. 2(b) and 2(c). Before the (1,5) mode grows large, it and the plasma rotate continuously. The same is true for the other $m=1$ modes (not shown). However, as the (1,5) mode amplitude becomes large, this mode and the bulk plasma, represented by the CV ions, slow down. CV rotation is taken as representative of bulk plasma rotation in the core, since the CV ions and $m=1$ modes always rotate at similar velocities.²⁶ Eventually, at 19 ms, the (1,5) mode, as well as the other $m=1$ modes, locks and remains locked until the end of the discharge (which occurs at 47 ms in this case). The plasma does not cease to rotate, however, but continues on at a reduced speed, as is typical with mode locking in MST. Such permanent mode locking is the typical result of QSH mode growth and braking, as long as the mode grows to sufficient amplitude. However, the modes and plasma do occasionally spin up again, after the dominant mode amplitude has dropped. There are also plasmas in which the dominant mode amplitude drops during the mode deceleration before locking can occur. In these cases, the modes and plasma reaccelerate.

The appearance of the QSH mode spectrum and the resultant braking and locking has little effect on the global equilibrium. This is in contrast to locking in the tokamak, which often results in a disruption. The MST plasma does

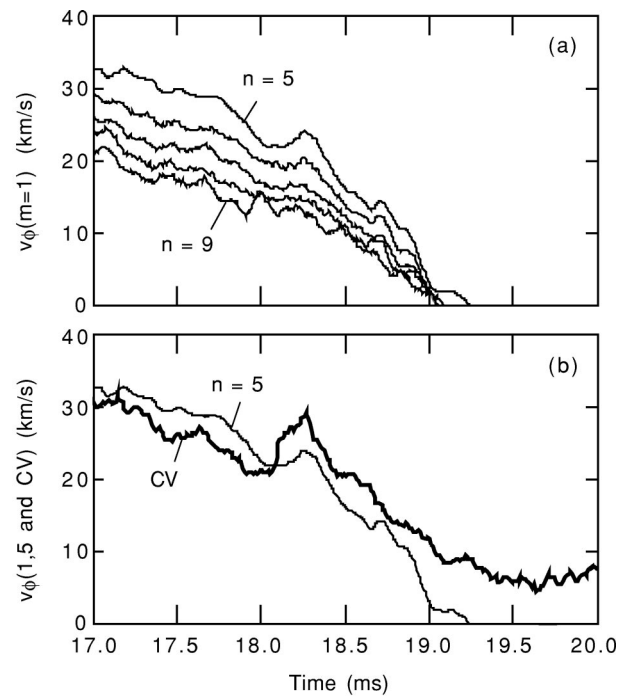


FIG. 3. From the $F=0$ plasma used in Fig. 1, (a) toroidal phase velocity of the $m=1, n=5-9$ modes, in order from top to bottom, and (b) the toroidal phase velocity of the $m=1, n=5$ mode and toroidal flow velocity of the CV ions.

not disrupt in the presence of such a large mode partly because the field structure in the core of a standard RFP plasma is already stochastic, although the region within the large mode's island is substantially less stochastic, possibly exhibiting healed flux surfaces.²³ To illustrate the constancy of the plasma equilibrium in QSH plasmas, we show the toroidal plasma current and line-averaged electron density in Figs. 1(d) and 1(e). Parameters such as F and Θ , which reflect the shape of the magnetic field profiles,²⁷ are also unchanging.

The deceleration and locking of the $m=1, n=5-9$ modes in the plasma shown in Fig. 2 are shown in detail in Fig. 3(a). In Fig. 3(b), we overlay the (1,5) and CV velocities. Since each tearing mode rotates with a velocity determined by the plasma flow in the vicinity of the mode's resonant surface, differing mode velocities reflect a radial variation of the plasma flow velocity. While the radial profile of the flow varies somewhat shot to shot (e.g., some profiles are flatter than others), a feature common to all plasmas in this study is that the core-resonant $m=1$ modes and CV ions decelerate on the same time scale. This is sensible since the mode resonant surfaces and CV ions overlap in space.

With the data shown thus far, we have established a clear correlation between the growth of the QSH dominant mode and the mode (and plasma) deceleration. When the QSH spectrum appears, the mode phase velocity evolves as a relatively simple function of the mode amplitude. In Fig. 4 we plot the mode phase velocity versus the normalized mode amplitude extracted from 10 to 20 ms from the data shown in Fig. 2. The mode amplitude is normalized to the equilibrium field strength at the plasma boundary. Henceforth, we will refer to curves such as that shown in Fig. 4 as braking

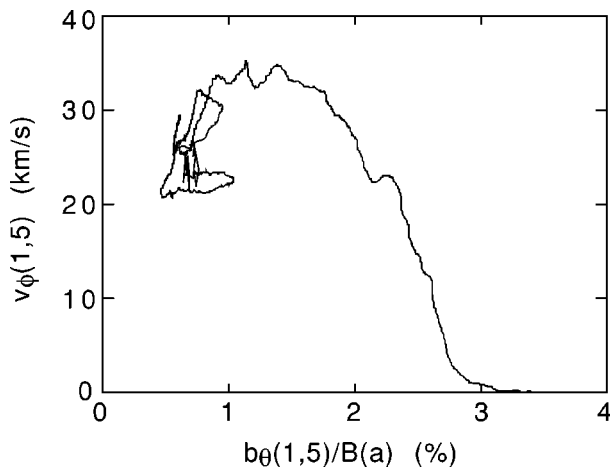


FIG. 4. From poloidal magnetic fluctuation measurements, the (1,5) toroidal phase velocity versus the normalized mode amplitude. Data was extracted from 10 to 20 ms from the shot shown in Fig. 2. A 250- μ s smooth is applied to the data.

curves. At low mode amplitude in Fig. 4, the velocity is largely independent of amplitude, but as the mode amplitude grows, a clear relation between velocity and amplitude emerges, with the velocity steadily decreasing until locking occurs. The braking curve is not perfectly smooth due to both noise in the data and real variations in the mode amplitude and velocity. Curves like that shown in Fig. 4 are traced out whenever the QSH dominant mode grows to sufficient amplitude. More braking curves are shown below.

In this section, we have shown that braking and locking of the core-resonant $m=1$ modes accompany the growth to large amplitude of the innermost resonant $m=1$ mode. We have also demonstrated that this mode braking is accompanied by deceleration of the bulk plasma. In the next section, we begin examination of the possible causes of this mode braking.

III. ROLE OF THE ERROR FIELD AND MODE COUPLING

There are previously established mechanisms for mode braking and locking in MST that could, in principle, contribute to the phenomenology described above. One mechanism is the torque exerted by error fields. Another is the torque exerted via nonlinear coupling to other modes resonant in the plasma. We will show that neither mechanism plays a role here.

A. Error field

As with the torque from eddy currents in the shell, the torque from an error field is exerted on the plasma in the vicinity of a tearing mode's resonant surface and is proportional to the product of the mode's amplitude and the corresponding resonant component of the error field.^{8,18} It has been demonstrated in MST that a sufficiently large $m=1$ error field applied at the poloidal gap can decelerate and lock the $m=1$ modes.¹⁷ Given the large amplitude to which the QSH dominant mode grows, even a relatively small error

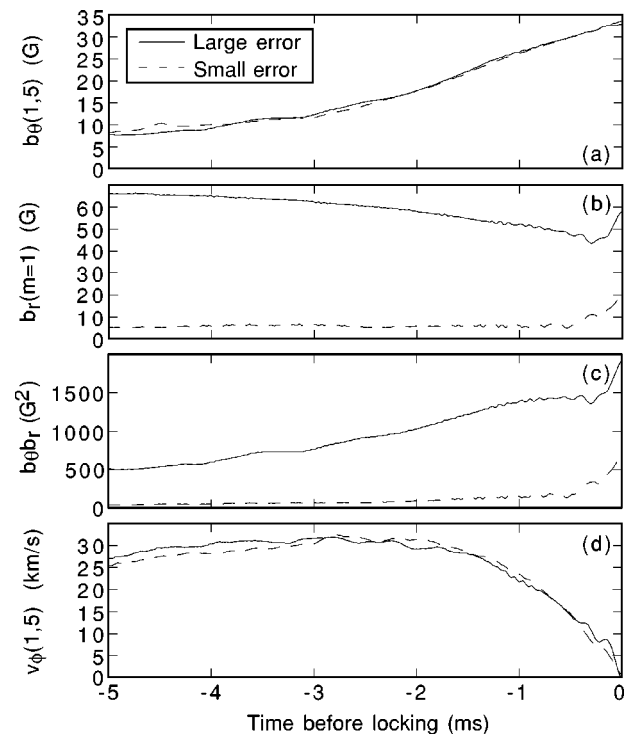


FIG. 5. In the presence of large and small error fields, time variations of (a) the poloidal magnetic fluctuation amplitude of the (1,5) mode, (b) the amplitude of the $m=1$ radial error field at the poloidal gap, (c) the product of the mode amplitude and error field, and (d) the toroidal phase velocity of the (1,5) mode. Data were recorded on 8 January 2003.

might induce locking or, at least, affect the shape of the braking curve. There is a finite error field at the poloidal gap in all the plasmas studied here.

To test for influence of the error field, we examined QSH mode braking with an $m=1$ error field of varying magnitude. The error field magnitude can be varied shot to shot. Shot-averaged wave forms from plasmas with a QSH mode spectrum but differing error fields are shown in Fig. 5. One ensemble is comprised of seven shots with a large error field, and the other is comprised of eight shots with a small error field. The ensembles are comprised of data extracted from each shot during the 5-ms interval leading up to locking of the dominant mode. These $F=0$ plasmas were generated on the same day with the same plasma current and similar electron density. The (1,5) mode amplitude and the amplitude of the $m=1$ radial error field are shown in Figs. 5(a) and 5(b). The two mode growth rates are very similar, showing that the mode growth is unaffected by the substantial difference in error field amplitude. The product of the mode and error-field amplitudes is shown in Fig. 5(c), showing that there is a large difference in the error-field torque in these plasmas. Even with this large difference, the evolution of the (1,5) velocity in the two cases, Fig. 5(d), is quite similar, even during the phase of rapid deceleration when the product of the mode and error-field amplitudes differs by almost an order of magnitude.

Not surprisingly, given the data in Fig. 5, there is no significant difference in the braking curves for these two ensembles. In Fig. 6 we show two shot-averaged QSH braking

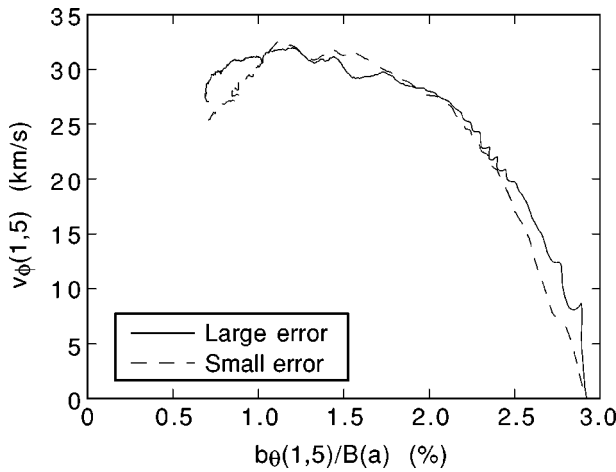


FIG. 6. Shot-averaged braking curves for the (1,5) mode in the presence of large and small error fields. Curves were compiled from the same plasmas as those used in Fig. 5.

curves, comprised of data from the same ensembles used in Fig. 5. Not only are the shapes of these curves quite similar, but the value of the mode amplitude at which locking occurs is the same. The similarity of the braking curves is also apparent when one compares individual shots (i.e., this similarity is not an artifact of averaging). We did record some plasmas with an error field much larger than that shown in Fig. 5(b). Consistent with previous experiments,¹⁷ an error field well over 100 G caused robust locking of the $m=1$ modes, in most cases in the absence of a QSH spectrum. Although the error field is unimportant within the range of error amplitude shown in Fig. 5, we did adjust the error field to be as small as possible in the plasmas modeled below.

B. Mode coupling

In addition to the error field, there is also a torque that can be exerted by other resonant tearing modes.^{18,28} This torque is exerted via nonlinear coupling of three modes, one of which is the QSH dominant mode. In contrast to the externally imposed torque due to an error field or eddy currents in the shell, which causes a net loss of plasma angular momentum, the torque from mode coupling results only in a redistribution of momentum *internal* to the plasma. The most important three-wave-coupled triplet for this paper involves modes with $(m,n)=(1,n_{QSH}), (1,n_{QSH}+1),$ and $(0,1)$. The torque is proportional to the product of the three mode amplitudes and, once again, is exerted on the plasma in the vicinity of each mode's resonant surface. When substantial, this mutual torque causes the $m=1$ and $m=0$ mode phase velocities to equilibrate. In MST plasmas, the $m=0$ modes are either stationary in the laboratory frame or rotate in the direction opposite the $m=1$ modes. Thus, when nonlinear coupling is substantial, the $m=1$ modes decelerate.

Obvious evidence for this coupling and equilibration has previously been observed only during sawtooth crashes, when both the $m=1$ and $m=0$ mode amplitudes become quite large for a brief time.²⁸ Between crashes, when mode amplitudes are generally smaller, the coupling is very weak.²⁸ In this study, we exclude plasmas in which a saw-

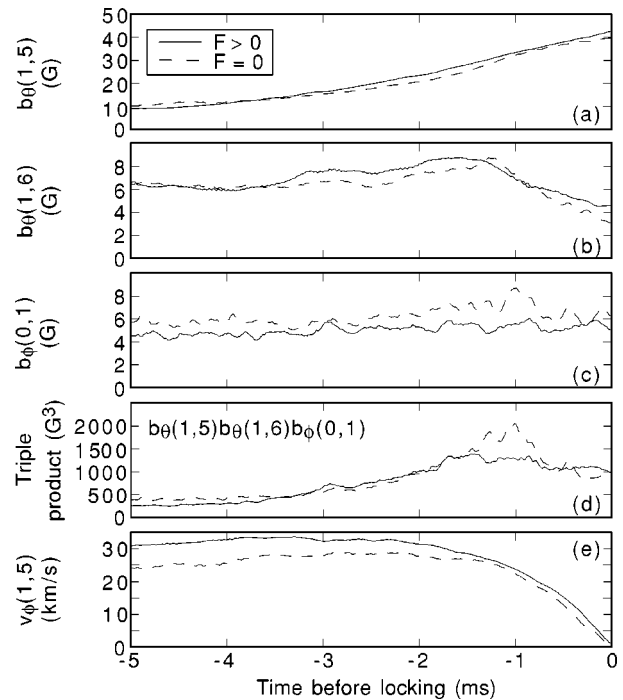


FIG. 7. In $F>0$ and $F=0$ plasmas, time variations of the poloidal magnetic fluctuation amplitude of the (a) (1,5) mode and (b) (1,6) mode, (c) the toroidal magnetic fluctuation amplitude of the (0,1) mode, (d) the product of the (1,5), (1,6), and (0,1) mode amplitudes, and (e) the toroidal phase velocity of the (1,5) mode. Data were recorded on 30 March 2001 and 3 April 2001.

tooth crash occurs during deceleration of the QSH dominant mode. Between crashes in QSH plasmas, as in other standard MST plasmas, the amplitude of the (0,1) mode is small. Thus we expect that the three-wave torque is also small.

We demonstrate that the torque is small in $F=0$ plasmas by comparing braking of the (1,5) QSH mode in $F=0$ and $F>0$ plasmas. In $F=0$ plasmas, the (0,1) mode is resonant at the plasma boundary at the inner surface of MST's thick conducting shell. In $F>0$ plasmas, $q>0$ everywhere in the plasma, excluding the $m=0$ resonant surface from the plasma and eliminating the three-wave torque. In Fig. 7 are data from two shot ensembles, one comprised of 11 shots with $F=0$ and the other comprised of 19 shots with $F=+0.015$. These discharges all had the same plasma current, similar electron density, and the same (small) $m=1$ error field. The amplitudes of the (1,5), (1,6), and (0,1) modes are compared in Figs. 7(a)–7(c). The evolution of the $m=1$ modes is quite similar comparing the two cases. The amplitude of the (0,1) mode in the $F>0$ case represents a baseline or noise level since the mode is not resonant in the plasma. The (0,1) amplitude in the $F=0$ plasmas is just slightly above the baseline. The product of the three mode amplitudes is compared in Fig. 7(d). Except for a brief time, the product in the $F=0$ ensemble differs very little from that in the $F>0$ ensemble, the latter reflecting a baseline in the triple product and three-wave torque. The evolution of the (1,5) velocity in the two cases is quite similar, Fig. 7(e), although the initial velocity differs due to the slightly different equilibria.

The two shot-averaged braking curves for these data are

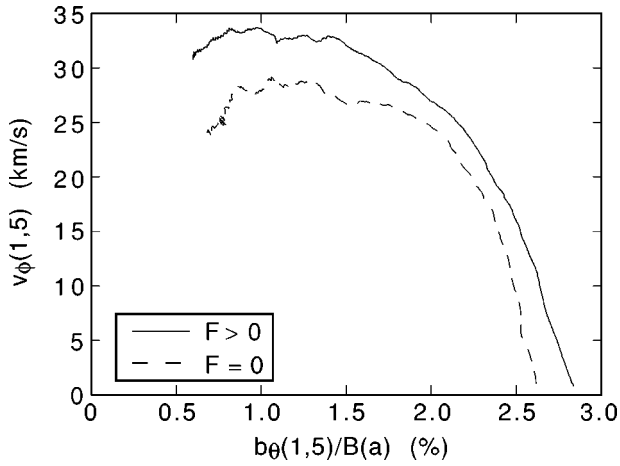


FIG. 8. Shot-averaged braking curves for the (1,5) mode in $F > 0$ and $F = 0$ plasmas. Curves were compiled from the same plasmas as those used in Fig. 7.

shown in Fig. 8. There is an offset between the two curves that arises due to differences in both the phase velocities and mode amplitudes. The difference in phase velocities originates before braking begins. Although the offset in the curves exists all the way to locking, the shapes of the braking curves are quite similar (i.e., the rate of deceleration is quite similar). The similarity of the mode amplitude triple products and the braking curves allows one to conclude that the three-wave torque is small during braking in $F = 0$ plasmas.

IV. TIME-INDEPENDENT MODELING

Having ruled out other, previously established causes of braking and locking in MST to explain the braking shown in Sec. II, we turn to the torque exerted by eddy currents flowing in the conducting shell. An RFP-specific model for this effect was described in Ref. 9. In this section, we first describe the model, which is time independent in that it assumes a mode amplitude—and thus an eddy-current torque—that evolves on a time scale much, much slower than that of the mode deceleration. Most of the equations shown in this section are taken directly from Ref. 9. In describing the braking curve predicted by this model for MST, we note a significant correction to the curve. The corrected curve predicts braking due to eddy currents at a substantially smaller mode amplitude. In Sec. V, we describe the time-dependent extension to the model, made necessary by the violation of the time-independent assumption in the plasmas studied here. We then show applications of the time-dependent model to experimental data and discuss the degree to which the model fits the data.

A. Geometry and equilibrium

The model assumes large aspect ratio and zero β_p (the volume-integrated plasma pressure normalized to the poloidal magnetic field pressure at the plasma boundary). Hence, the equilibrium is well approximated as a periodic cylinder, and cylindrical polar coordinates (r, θ, z) are adopted. The major and minor radii of the cylindrical model plasma are R_0 and a . A simulated toroidal angle is defined as $\phi = z/R_0$. The

system is assumed to be periodic in the z direction, with periodicity length $2\pi R_0$. MST's conducting shell is assumed to be uniform in the axial and azimuthal (toroidal and poloidal) directions. The fact that the actual shell has portholes and two gaps should not significantly affect the results, since the induction of eddy currents does not require a completely continuous conductor, as noted recently in a tokamak with a segmented shell.²⁹

Internal magnetic field profiles are modeled according to the standard, well-tested $\alpha - \theta_0$ equilibrium model,²⁷ according to which

$$\nabla \times \mathbf{B} = \sigma(r)\mathbf{B}, \quad (1)$$

where

$$\sigma = \left(\frac{2\theta_0}{a} \right) \left[1 - \left(\frac{r}{a} \right)^\alpha \right], \quad (2)$$

and θ_0 and α are positive constants. The experimental inputs to this equilibrium model are the reversal and pinch parameters, F and Θ , measured at the plasma boundary.

B. Perturbed magnetic field

The model assumes only one unstable core-resonant $m = 1$ tearing mode. The magnetic perturbation associated with the single (m, n) mode is

$$\mathbf{b}(\mathbf{r}) = \mathbf{b}(r)e^{i(m\theta - n\phi)}, \quad (3)$$

where

$$b_r^{m,n} = \frac{i\psi}{r}, \quad (4)$$

$$b_\theta^{m,n} = -\frac{m\psi'}{m^2 + n^2\epsilon^2} + \frac{n\epsilon\sigma\psi}{m^2 + n^2\epsilon^2}, \quad (5)$$

$$b_\phi^{m,n} = \frac{n\epsilon\psi'}{m^2 + n^2\epsilon^2} + \frac{m\sigma\psi}{m^2 + n^2\epsilon^2}, \quad (6)$$

$\epsilon(r) = r/R_0$, and the prime denotes d/dr .

The linearized magnetic flux function $\psi(r) = \psi^{m,n}(r)$ satisfies Newcomb's equation³⁰

$$\frac{d}{dr} \left[f \frac{d\psi}{dr} \right] - g\psi = 0, \quad (7)$$

where

$$f(r) = \frac{r}{m^2 + n^2\epsilon^2}, \quad (8)$$

$$g(r) = \frac{1}{r} + \frac{r(n\epsilon B_\theta + mB_\phi)}{(m^2 + n^2\epsilon^2)(mB_\theta - n\epsilon B_\phi)} \frac{d\sigma}{dr} + \frac{2mn\epsilon\sigma}{(m^2 + n^2\epsilon^2)^2} - \frac{r\sigma^2}{m^2 + n^2\epsilon^2}. \quad (9)$$

Equation (7) is singular at the tearing mode's resonant surface, located at minor radius r_s , which satisfies

$$mB_\theta(r_s) - n\epsilon(r_s)B_\phi(r_s) = 0. \quad (10)$$

In the vacuum region (where $\sigma=0$) surrounding the plasma, the most general solution to Newcomb's equation takes the form

$$\psi = A i_m(n\epsilon) + B k_m(n\epsilon), \quad (11)$$

where A and B are arbitrary constants, and

$$i_m(n\epsilon) = |n\epsilon| I_{m+1}(|n\epsilon|) + m I_m(|n\epsilon|), \quad (12)$$

$$k_m(n\epsilon) = -|n\epsilon| K_{m+1}(|n\epsilon|) + m K_m(|n\epsilon|). \quad (13)$$

Here, I_m and K_m represent standard modified Bessel functions.

In this model, the tearing mode is purely a current-driven instability. The destabilizing effect of the experimentally finite plasma pressure is explicitly neglected. This is justified by the fairly flat pressure profile in the core of standard MST plasmas and the relatively small value of $\beta_p \sim 7\%$. Under these conditions, the contribution of pressure to core-resonant tearing instability is small.³¹

C. Standard tearing eigenfunctions

Let $\psi_s(r, d)$ represent the standard normalized tearing eigenfunction calculated assuming a perfectly conducting shell at minor radius d . In other words, $\psi_s(r, d)$ is a real solution to Newcomb's equation (7) which is well behaved as $r \rightarrow 0$ and satisfies

$$\psi_s(r_s, d) = 1, \quad (14)$$

$$\psi_s(r \geq d, d) = 0. \quad (15)$$

There are gradient discontinuities in $\psi_s(r, d)$ at $r = r_s$ and $r = d$. The quantity

$$E(d) = \left[r \frac{d\psi_s(r, d)}{dr} \right]_{r_{s-}}^{r_{s+}} \quad (16)$$

is the standard tearing stability index,³² calculated assuming a perfectly conducting shell at minor radius d .

D. Modified tearing eigenfunctions

Now assume a system with a finite-conductivity shell at minor radius b and a perfectly conducting shell at minor radius c , with $b < c$. The finite-conductivity shell imposes a modification on the standard tearing eigenfunction. The most general tearing eigenfunction is now written

$$\psi(r) = \Psi_s \psi_s(r, b) + \Psi_b \psi_b(r, b, c), \quad (17)$$

where Ψ_s and Ψ_b are complex parameters which determine the amplitude and phase of the tearing perturbation at the rational surface and finite-conductivity shell, respectively. The normalized eigenfunction $\psi_b(r, b, c)$ is a real solution to Newcomb's equation which is well behaved as $r \rightarrow 0$ and satisfies

$$\psi_b(r_s, b, c) = 0, \quad (18)$$

$$\psi_b(b, b, c) = 1, \quad (19)$$

$$\psi_b(c, b, c) = 0. \quad (20)$$

It is nonzero only in the radial range $r_s < r < c$, and it possesses gradient discontinuities at $r = r_s$, $r = b$, and $r = c$. This eigenfunction parametrizes the interaction between the tearing mode and eddy currents induced in the finite-conductivity shell, in the presence of the perfectly conducting shell.

E. Modified tearing dispersion relation

In the presence of the two shells, the dispersion relation for the tearing mode takes the form

$$\Delta \Psi_s = E(b) \Psi_s + E_{sb} \Psi_b, \quad (21)$$

$$\Delta \Psi_b = -\frac{E_{sb} E_{bs}}{E(c) - E(b)} \Psi_b + E_{bs} \Psi_s, \quad (22)$$

where

$$\Delta \Psi_s = \left[r \frac{d\psi}{dr} \right]_{r_{s-}}^{r_{s+}} \quad (23)$$

is a complex parameter which determines the amplitude and phase of the eddy currents induced in the vicinity of the tearing mode's resonant surface, and

$$\Delta \Psi_b = \left[r \frac{d\psi}{dr} \right]_{b-}^{b+} \quad (24)$$

is a complex parameter which determines the amplitude and phase of the eddy currents induced in the finite-conductivity shell. Furthermore,

$$E_{sb} = \left[r \frac{d\psi_b(r, b, c)}{dr} \right]_{r_{s+}} \quad (25)$$

and

$$E_{bs} = -\left[r \frac{d\psi_s(r, b)}{dr} \right]_{b-} \quad (26)$$

are both real parameters.

From Newcomb's equation (7) one can demonstrate that

$$(m^2 + n^2 \epsilon_b^2) E_{sb} = (m^2 + n^2 \epsilon_s^2) E_{bs}, \quad (27)$$

where $\epsilon_b = b/R_0$ and $\epsilon_s = r_s/R_0$. One can also demonstrate that

$$\psi_b(r, b, c) = \frac{E_{sb}}{E(c) - E(b)} [\psi_s(r, c) - \psi_s(r, b)]. \quad (28)$$

In the vacuum region outside the plasma,

$$\psi_s(r, b) = \begin{cases} \psi_s(a, b) \frac{k_m(n\epsilon_b) i_m(n\epsilon) - k_m(n\epsilon) i_m(n\epsilon_b)}{k_m(n\epsilon_b) i_m(n\epsilon_a) - k_m(n\epsilon_a) i_m(n\epsilon_b)}, & a \leq r \leq b, \\ 0, & r > b, \end{cases} \quad (29)$$

where $\epsilon_a = a/R_0$. It follows from Eqs. (26) and (27) that

$$E_{bs} = \frac{\psi_s(a,b)(m^2 + n^2 \epsilon_b^2)}{k_m(n\epsilon_b)i_m(n\epsilon_a) - k_m(n\epsilon_a)i_m(n\epsilon_b)}, \quad (30)$$

$$E_{sb} = \frac{\psi_s(a,b)(m^2 + n^2 \epsilon_s^2)}{k_m(n\epsilon_b)i_m(n\epsilon_a) - k_m(n\epsilon_a)i_m(n\epsilon_b)}. \quad (31)$$

Thus, all of the real parameters appearing in the modified tearing dispersion relation (21) and (22) [i.e., $E(b)$, $E(c)$, E_{bs} , and E_{sb}] can be calculated knowing the standard tearing eigenfunction $\psi_s(r,d)$.

F. Shell physics

Given a shell with radius b , radial thickness δ_b , and electrical conductivity σ_b , the shell time constant is defined

$$\tau_b = \mu_0 \sigma_b \delta_b b. \quad (32)$$

The conducting shell in MST is sufficiently thick that the rotating tearing perturbation amplitude is zero outside the shell (at $r > b + \delta b$). The shell provides very strong shielding. Given this, one can write a dispersion relation for the vacuum vessel,

$$\Delta \Psi_b = \left(in \Omega_s \tau_b \frac{b}{\delta_b} \right)^{1/2} \Psi_b, \quad (33)$$

relating the amplitude and phase of the eddy currents induced in the finite-conductivity shell to the amplitude and phase of the tearing perturbation at the same location. Introduced in this expression is Ω_s , the toroidal angular velocity of the plasma at the tearing mode resonant surface. It is assumed that the tearing mode and plasma corotate toroidally at the mode's resonant surface. This is commonly referred to as the *no-slip* constraint. The plasma's toroidal angular velocity profile is represented by $\Omega(r)$.

From Eqs. (21), (22), and (33), one can also derive the dispersion relation at the resonant surface,

$$\Delta \Psi_s \approx e^{-i\pi/4} \frac{E_{sb} E_{bs}}{(n\Omega_s \tau_b b / \delta_b)^{1/2}} \Psi_s + E(b) \Psi_s, \quad (34)$$

relating the amplitude and phase of the eddy currents induced in the vicinity of the mode's resonant surface to the amplitude and phase of the tearing perturbation at the same location.

G. Electromagnetic torque

This braking model includes both the electromagnetic braking torque exerted between the finite-conductivity shell and local plasma in the vicinity of the mode's resonant surface, and the viscous restoring torque exerted between the local plasma and exterior bulk plasma. The toroidal electromagnetic torque acting in the vicinity of the resonant surface due to eddy currents flowing in the conducting shell is given by

$$\delta T_{EM} = \frac{2\pi^2 R_0}{\mu_0} \frac{n}{m^2 + n^2 \epsilon_s^2} \text{Im}\{\Delta \Psi_s (\Psi_s)^*\} \quad (35)$$

or

$$\delta T_{EM} \approx - \frac{\pi^2 R_0 \sqrt{2}}{\mu_0} \frac{n |\Psi_s|^2}{m^2 + n^2 \epsilon_s^2} \frac{E_{sb} E_{bs}}{(n\Omega_s \tau_b b / \delta_b)^{1/2}}. \quad (36)$$

In general, the electromagnetic torque has a dependence on the phase lag φ at the mode resonant surface between the tearing perturbation and the perturbation induced by the eddy currents flowing in the shell (or, equivalently, the phase lag at the shell between the tearing perturbation and induced eddy currents). This dependence is $\sin \varphi$, meaning that, all else being equal, the electromagnetic torque is largest for a phase lag of $\pi/2$ and smallest (zero) for a phase lag of 0. This phase lag depends on the mode angular velocity (rotation frequency).

To understand the origin of the phase lag and its dependence on angular velocity, consider the shell to be a driven L/R circuit characterized by

$$L \frac{dI}{dt} + RI = V_0 e^{i\omega t}, \quad (37)$$

where I is the eddy current induced in the shell, V_0 is the mode amplitude, and ω is the mode rotation frequency. In steady state (with I and V_0 oscillating at the same frequency),

$$I = \frac{V_0/R}{1 + i\omega L/R}. \quad (38)$$

The phase between V_0 and I is

$$\varphi = \tan^{-1} \left[\frac{-\omega L}{R} \right] = \tan^{-1} \left[\frac{-\omega}{(R/L)} \right], \quad (39)$$

and L/R is the shell (circuit) time constant. Hence,

$$\varphi \rightarrow \begin{cases} \pi/2, & \omega \gg R/L, \\ 0, & \omega \ll R/L. \end{cases} \quad (40)$$

In the time-independent modeling described in this section, the phase lag is approximated to be a constant $\pi/4$, independent of mode velocity. In the time-dependent modeling described in the next section, the full variation of the phase lag with mode velocity is included.

H. Viscous torque

The steady-state change in the plasma toroidal angular velocity induced by δT_{EM} is written

$$\Delta \Omega(r) = \Delta \Omega_s \begin{cases} \int_r^a \frac{dr}{\mu r} / \int_{r_s}^a \frac{dr}{\mu r}, & r_s \leq r \leq a, \\ 1, & r < r_s, \end{cases} \quad (41)$$

where $\mu(r)$ is the plasma perpendicular viscosity profile and

$$\Delta \Omega_s = \Omega_s - \Omega_s^{(0)}. \quad (42)$$

Here, $\Omega_s^{(0)}$ is the value of Ω_s in the absence of eddy currents flowing in the shell. It is sometimes referred to as the "natural" angular velocity. The viscous restoring torque acting in the vicinity of the resonant surface is written

$$\delta T_{VS} = 4 \pi^2 R_0 \left[r \mu R_0^2 \frac{d\Delta\Omega}{dr} \right]_{r_{s-}}^{r_{s+}}. \quad (43)$$

It follows from Eqs. (41) and (42) that

$$\delta T_{VS} = 4 \pi^2 R_0^3 [\Omega_s^{(0)} - \Omega_s] \left/ \int_{r_s}^a \frac{dr}{\mu r} \right. \quad (44)$$

I. Torque balance

In this time-independent (steady-state) model, the electromagnetic and viscous restoring torques are exactly balanced—i.e.,

$$\delta T_{EM} + \delta T_{VS} = 0. \quad (45)$$

Hence, from Eqs. (36) and (44), one can write

$$\frac{\sqrt{27}}{2} \left(\frac{\Omega_s}{\Omega_s^{(0)}} \right)^{1/2} \left(1 - \frac{\Omega_s}{\Omega_s^{(0)}} \right) = \left(\frac{b_s}{\Lambda'' B_0} \right)^2, \quad (46)$$

where

$$b_s = \frac{|\Psi_s|}{r_s} \quad (47)$$

is the perturbed radial magnetic field strength at the mode's resonant surface due to the tearing perturbation,

$$\Lambda'' = \left[\frac{4\sqrt{2}}{\sqrt{27}} \frac{\tau_H^2 (n\Omega_s^{(0)})^{3/2} (\tau_b b / \delta_b)^{1/2} m^2 + n^2 \epsilon_s^2}{\tau_V} \frac{m^2 + n^2 \epsilon_s^2}{n^2 \epsilon_s^2} \right. \\ \left. \times \frac{1}{E_{sb} E_{bs}} \left/ \int_{r_s}^a \frac{\mu(0)}{\mu(r)} \frac{dr}{r} \right. \right]^{1/2}, \quad (48)$$

and B_0 is the equilibrium magnetic field strength. In Eq. (48),

$$\tau_H = \frac{a \sqrt{\mu_0 \rho_0}}{B_0} \quad (49)$$

is the typical hydromagnetic time scale,

$$\tau_V = \frac{a^2 \rho_0}{\mu(0)} \quad (50)$$

is the typical viscous diffusion time scale, and ρ_0 is the central plasma mass density. Equation (46) is used to generate theoretical braking curves.

J. Estimate of the plasma viscosity

To generate a theoretical braking curve, one needs an estimate of the plasma viscosity profile. Suppose that the viscosity profile takes the form

$$\mu(r) = \begin{cases} \infty, & r < r_c, \\ \mu_c, & r_c \leq r \leq a. \end{cases} \quad (51)$$

In other words, there is zero momentum confinement in the stochastic RFP plasma core, $r < r_c$, but finite momentum confinement outside this region. Suppose further that the intrinsic plasma rotation at the edge is negligibly small [$\Omega^{(0)}(a) \approx 0$] and that all of the toroidal momentum input to

the plasma occurs in the core. The model does not specify—nor does it depend on—the source(s) of viscosity or momentum. Thus, one derives

$$\Omega^{(0)}(r) = \Omega_c^{(0)} \begin{cases} 1, & r < r_c, \\ \ln(r/a) / \ln(r_c/a), & r_c \leq r \leq a. \end{cases} \quad (52)$$

The plasma rotation is constant in the plasma core and highly sheared in the outer region.

The viscous diffusion time scale (50) can be redefined

$$\tau_V = \frac{a^2 \rho_0}{\mu_c}, \quad (53)$$

reflecting the fact that the (finite) rate of viscous momentum diffusion out of the plasma is determined by the finite viscosity in the outer region of the plasma. Suppose that the plasma radial density profile is uniform. It follows that the global momentum confinement time τ_M , defined as the ratio of the net plasma toroidal angular momentum to the toroidal angular momentum injection rate, is related to τ_V via

$$\tau_V = -\tau_M \frac{a^3 [d\Omega^{(0)}(a)/dr]}{\int_0^a \Omega^{(0)} r dr}. \quad (54)$$

Hence,

$$\tau_V = \frac{4 \tau_M}{1 - (r_c/a)^2}. \quad (55)$$

Assume now that

$$\tau_M \approx \tau_E, \quad (56)$$

where τ_E is the global energy confinement time (the validity of this assumption is discussed in the next section). It then follows that

$$\tau_V \int_{r_s}^a \frac{\mu(0)}{\mu(a)} \frac{dr}{r} \rightarrow \kappa \tau_E \quad (57)$$

in Eq. (48), where

$$\kappa = \frac{4 \ln(a/r_c)}{1 - (r_c/a)^2}. \quad (58)$$

Hence, the viscous momentum diffusivity is parametrized in terms of the global momentum confinement time (in the absence of an electromagnetic torque), and this is in turn taken equal to the global energy confinement time.

K. Time-independent braking curve for MST

MST is comprised of a single, finite-conductivity shell. Given the lack, of course, of a perfectly conducting shell, the minor radius c of the perfectly conducting shell in the preceding analysis takes the value ∞ . In other words, the perfectly conducting shell is now located infinitely far from the plasma.

A sample braking curve is shown in Ref. 9 for the (1,6) tearing mode, initially rotating in an $I_\phi = 340$ kA MST hydrogen plasma. The braking curve is generated from Eq. (46)

TABLE I. Some of the parameters needed in Eq. (46) for generation of the time-independent braking curve for MST, Fig. 9.

Parameter	Value
I_ϕ (kA)	340
$B_0 \equiv B_\theta(a) = \mu_0 I_\phi / 2\pi a$ (T)	0.13
F	-0.2
Θ	1.59
α	3.0
Θ_0	1.71
R_0 (m)	1.5
a (m)	0.51
b (m)	0.52
δ_b (m)	0.05
$\epsilon_a = a/R_0$	0.34
r_s (m)	0.17
$\epsilon_s = r_s/R_0$	0.11
$1/\sigma_b$ (Ω m)	4.0×10^{-8}
n_{e0} (10^{19} m $^{-3}$)	1.0
$\tau_M = \tau_E$ (ms)	1.0

in the present paper. Some of the parameters needed for Eq. (46) are listed in Table I. Based on these parameters, one calculates

$$\tau_H = \frac{a \sqrt{\mu_0 m_p n_{e0}}}{B_0} = 5.5 \times 10^{-7} \text{ s} \quad (59)$$

and

$$\tau_b = \mu_0 \sigma_b \delta_b b = 0.82 \text{ s}. \quad (60)$$

Taking $V_\phi^{(0)}$, the initial plasma flow velocity in the vicinity of the mode's resonant surface, to be 10 km/s, one calculates

$$n\Omega_s^{(0)} = \frac{nV_\phi^{(0)}}{R_0} = 4 \times 10^4 \text{ rad/s}. \quad (61)$$

This is the angular velocity of the (1,6) mode in the limit of very low mode amplitude where the braking torque due to eddy currents is negligible.

For the chosen equilibrium (see Table I), Newcomb's equation provides $E(b) = 1.038$, $E(c) = 17.59$, $E_{bs} = 5.826$, and $E_{sb} = 1.614$. Taking the radius of the stochastic plasma core to be $r_c = 0.7a$, one calculates

$$\kappa = \frac{4 \ln(a/r_c)}{1 - (r_c/a)^2} = 2.8. \quad (62)$$

Using the above equations and parameter values allows one to calculate

$$\Lambda^n = \left[\frac{4\sqrt{2}}{\kappa\sqrt{27}} \frac{\tau_H^2 (n\Omega_s^{(0)})^{3/2} (\tau_b b / \delta_b)^{1/2} m^2 + n^2 \epsilon_s^2}{\tau_E n^2 \epsilon_s^2} \times \frac{1}{E_{sb} E_{bs}} \right]^{1/2} = 0.03. \quad (63)$$

To allow easier comparison with experimental data, b_s , the perturbed radial magnetic field strength at the mode's resonant surface due to the tearing perturbation, is related to the amplitudes of the poloidal and toroidal field perturbations at the location of MST's magnetic sensing coils via

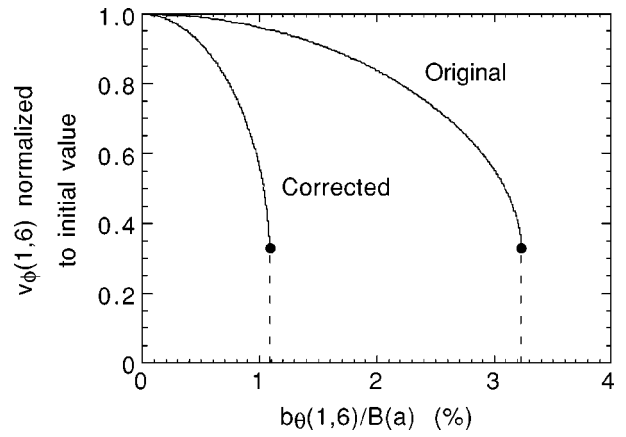


FIG. 9. Time-independent braking curves for MST based on Eq. (97) in Ref. 9. The curve labeled “Original” is the same curve found in Fig. 5 in that paper. The curve labeled “Corrected” is for the same plasma, but with a correction described in the present paper. Dots indicate the point on each curve across which the model predicts a discontinuous drop to very slow rotation.

$$b_{\theta b} = \frac{m}{m^2 + n^2 \epsilon_b^2} E_{bs} b_s \left(\frac{r_s}{b} \right), \quad (64)$$

$$b_{\phi b} = \frac{n \epsilon_b}{m^2 + n^2 \epsilon_b^2} E_{bs} b_s \left(\frac{r_s}{b} \right). \quad (65)$$

Note that the factor (r_s/b) ($\approx 1/3$ for MST) in both of these equations has been added as a correction to what was originally published in Eqs. (101) and (102) in Ref. 9.

Two braking curves generated from Eq. (46) are shown in Fig. 9. The curve labeled “Original” was generated using Eqs. (64) and (65) without the (r_s/b) correction factor. This is the curve that appears for MST in Fig. 5 of Ref. 9. The curve labeled “Corrected” in Fig. 9 incorporates the correction factor. Both curves represent a series of equilibria in which the electromagnetic and viscous torques are exactly balanced. One feature of these time-independent braking curves is the discontinuity that occurs when the mode velocity reaches about 1/3 of its initial value. Across this transition point, the braking torque due to eddy currents overwhelms the viscous restoring torque, and the mode's velocity is predicted to drop to a very low value.

Given the addition of the correction factor to Eqs. (64) and (65), the mode amplitude at which the transition to very slow rotation is predicted now drops from about 3% to about 1%, implying potentially wider applicability of this braking mechanism to MST plasmas. The same factor of r_s/b applies to Eqs. (115) and (116) in Ref. 9, applicable to the Reversed Field eXperiment (RFX) RFP that was in operation until 1999,³³ meaning that significant braking is also predicted at a lower mode amplitude in that device.

V. TIME-DEPENDENT MODELING

To model the braking data shown in Sec. II in terms of the torque exerted by eddy currents, we must add time dependence to the model. This is due to the fact that the mode amplitude (and the induced eddy currents) grows on the

same time scale as the mode deceleration. The time-dependent model is based on the same physics as the time-independent model.⁹ In this section, we describe the changes to the model necessitated by the addition of time dependence. We will also describe a few additional differences in the modeling not related to time dependence but pertinent to the MST plasmas studied in this paper. We then describe modeling for different MST plasmas and discuss the degree to which the model agrees with the experimental data. We will also illustrate why the addition of time dependence in the model is so important. We close this section with a brief discussion of mode locking.

A. Equilibrium and perturbed magnetic fields

Although time-dependent mode growth and braking are now accounted for, the plasma equilibrium is taken to be fixed during the mode deceleration. This is justified due to the constancy of F and Θ during the braking and due to data like that in Figs. 2(d) and 2(e). For each plasma modeled, the magnetic field profiles and, thus, the location of the QSH dominant mode's resonant surface are calculated 1 ms before locking occurs. We continue to use the α - Θ_0 model, but with a modification. Attempts to reconstruct, e.g., $F=0$ plasma equilibria assuming zero β_p failed in that the (1,5) mode was predicted to be barely nonresonant [$q(0) = 0.19$]. Hence, we reconstructed the plasma equilibrium using a more realistic finite- β version of the α - Θ_0 model. We take $\beta_p = 7\%$ for the $F=0$ plasmas and $\beta_p = 6.5\%$ for the $F = -0.2$ plasmas.^{21,34} Separate internal measurements of the magnetic field profiles in standard MST plasmas have shown good agreement with those reconstructed with this model.

We continue the assumption of only one unstable $m=1$ tearing mode. This is approximately justified for the QSH plasmas described here. The dominant $m=1$ mode in the QSH spectrum is substantially larger than the other $m=1$ modes [see Fig. 2(a)]. The other $m=1$ mode amplitudes are finite, meaning that these modes induce eddy currents in the conducting shell, but their amplitudes ($<1\%$ of the equilibrium field) are such that the corresponding braking torque is quite small. This is supported by the data in Fig. 4, which shows (for a single mode) no apparent relation between mode amplitude and velocity for amplitudes $<1\%$.

B. Time-dependent shell response

Given that $\delta_b \ll b$ for MST's conducting shell, Ohm's law yields within the shell

$$\mu_0 \sigma_b \frac{\partial \psi}{\partial t} = \frac{\partial^2 \psi}{\partial r^2}. \quad (66)$$

The boundary conditions on $\psi(r, t)$ are

$$\psi(b, t) = \Psi_b(t), \quad (67)$$

$$\left(\frac{\partial \ln \psi}{\partial \ln r} \right)_{r=b+\delta_b} = \zeta, \quad (68)$$

where $\Psi_b(t)$ is the perturbed magnetic flux at the inner boundary of the shell, and

$$\zeta = \left[\frac{d \ln k_m(n \epsilon)}{d \ln(r)} \right]_{r=b}. \quad (69)$$

The (complex) *shell response function* is defined as

$$G(t) = - \left(\frac{\partial \ln \psi}{\partial \ln r} \right)_{r=b} + \zeta. \quad (70)$$

Equations (66)–(68) can be solved to give

$$G(t) = \sqrt{\frac{\gamma \tau_b}{\delta}} \tanh(\sqrt{\gamma \tau_b \delta}) - \frac{1}{\delta} \sum_{j=1, \infty} f_j, \quad (71)$$

where $\gamma(t) = d \ln \Psi_b / dt$ is the (complex) growth rate of the shell flux, $\delta = \delta_b / b$, and

$$\frac{df_j}{dt} = -(\lambda_j + \gamma) f_j + \sigma_j \frac{d\gamma}{dt}, \quad (72)$$

with

$$\lambda_j = \frac{(j-1/2)^2 \pi^2}{\tau_b \delta}, \quad (73)$$

$$\sigma_j = \frac{2\lambda_j}{(\gamma + \lambda_j)^2}. \quad (74)$$

The above expressions were derived given that the conditions $|\gamma| \tau_b \gg \delta$ and $\lambda_j \tau_b \gg \delta$ are both satisfied in MST. The first term on the right-hand side of Eq. (71) represents the *steady-state* response of the shell, whereas the second term represents the *transient* response.

C. Time-dependent electromagnetic torque

The electromagnetic torque induced by the rotating mode now varies in time due both to the growing mode amplitude and to the decelerating mode velocity. The toroidal electromagnetic torque acting in the vicinity of the mode resonant surface takes the form

$$T(t) = - \frac{2\pi^2 R_0}{\mu_0} \frac{n}{m^2 + n^2 \epsilon_s^2} E_{sb} E_{bs} |\Psi_s|^2 \frac{\text{Im}[G(t)]}{|G(t) + \kappa|^2}, \quad (75)$$

where

$$\kappa = \frac{E_{sb} E_{bs}}{E(c) - E(b)}. \quad (76)$$

Let

$$\Psi_s = |\Psi_s| e^{i\varphi_s}, \quad (77)$$

where φ_s is the helical phase of the tearing mode. It follows that

$$\gamma(t) = \frac{d \ln |\Psi_s|}{dt} + i \frac{d\varphi_s}{dt} - \frac{dG(t)/dt}{G(t) + \kappa}. \quad (78)$$

Finally, the no-slip constraint at the resonant surface yields

$$\frac{d\varphi_s(t)}{dt} = n\Omega(r_s, t). \quad (79)$$

D. Time-dependent viscous response

The viscosity in the present model is now taken to be finite, and constant, across the entire plasma. This is consistent with measurements made in MST.³⁵ The viscosity is also taken to be constant in time, but the viscous torque evolves with the changing plasma rotation. The plasma momentum diffusivity is once again parametrized in terms of the global momentum confinement time (in the absence of braking torque).

The plasma toroidal equation of motion is written

$$r\rho \frac{\partial \Delta\Omega}{\partial t} - \mu \frac{\partial}{\partial r} \left(r \frac{\partial \Delta\Omega}{\partial r} \right) = \frac{T(t)}{4\pi^2 R_0^3} \delta(r-r_s), \quad (80)$$

where $\Delta\Omega = \Omega - \Omega^{(0)}$, $\Omega^{(0)}(r)$ is the unperturbed toroidal rotation profile, and μ is the viscosity. The plasma density ρ is once again assumed to be uniform. The boundary conditions associated with the above equation are

$$\frac{\partial \Delta\Omega(0,t)}{\partial r} = \Delta\Omega(a,t) = 0. \quad (81)$$

Subject to these boundary conditions, Eq. (80) can be solved to give

$$\Omega(r_s, t) = \Omega^{(0)}(r_s) + \sum_{n=1,\infty} g_n(t), \quad (82)$$

where

$$\frac{dg_n}{dt} = -\beta_n g_n + \frac{T(t)[u_n(r_s)]^2}{4\pi^2 R_0^3 a^2 \rho}. \quad (83)$$

Here,

$$u_n(r) = \sqrt{2} \frac{J_0(j_{0,n}r/a)}{J_1(j_{0,n})} \quad (84)$$

and

$$\beta_n = \frac{\mu}{\rho a^2} j_{0,n}^2. \quad (85)$$

Note that $j_{0,n}$ is the n th zero of the J_0 Bessel function and that the momentum confinement time is written $\tau_M = 1/\beta_1$.

Equations (71), (72), (75), (78), (79), (82), and (83) form a closed set. They can be used to determine the temporal variation of the tearing mode phase velocity, $d\varphi_s/dt$, given the temporal variation of the mode amplitude, $|\Psi_s|$. Note that the amplitudes of the perturbed poloidal and toroidal fields at the location of MST's magnetic sensing coils are

$$|b_\theta(t)| = \frac{m}{m^2 + n^2 \epsilon_b^2} \frac{E_{sb}}{b} \frac{|G - \zeta|}{|G + \kappa|} |\Psi_s|, \quad (86)$$

$$|b_\phi(t)| = \frac{n \epsilon_b}{m^2 + n^2 \epsilon_b^2} \frac{E_{sb}}{b} \frac{|G - \zeta|}{|G + \kappa|} |\Psi_s|. \quad (87)$$

E. Time-dependent braking curves

Experimental and (time-dependent) model braking curves for three different plasma types are shown in Fig. 10.

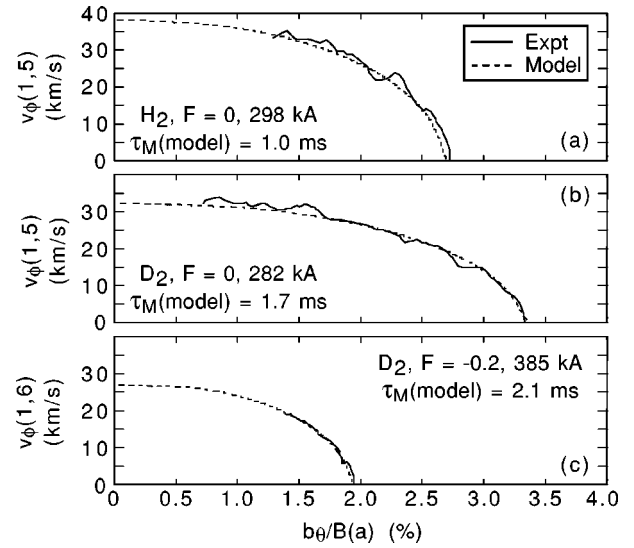


FIG. 10. Experimental and model braking curves for three different plasma types. Indicated in each figure are the fuel isotope, toroidal magnetic field reversal parameter, and toroidal plasma current. Also indicated are the model-predicted values of the global momentum confinement time. From top to bottom, these data are from shots (1990131033, 1990201021, and 1001112138).

The parameters fed into the model to generate the theoretical curves are essentially the same as those described for Eq. (46), from which the time-independent braking curve was generated. Two differences are that the time-dependent mode amplitude, $b_s \propto b_\theta$, and the initial mode velocity, $\Omega_s^{(0)} \propto v_\phi^{(0)}$, are now taken directly from experimental measurements. The growth rate of b_θ varies from plasma to plasma, but in all cases studied here, the mode growth is approximately linear versus time ($b_\theta \sim t$). Since b_θ never reaches zero in the experiment, each experimental braking curve is extrapolated to zero mode amplitude to determine $v_\phi^{(0)}$. The uncertainty introduced by this extrapolation is minimal.

A third difference between the present modeling and that described in the previous section is that the value of $\tau_v \propto \tau_M$ appearing in Eq. (48) is no longer assumed. Instead, the model is used to *predict* τ_M . The momentum confinement time is the single adjustable parameter in the model, and it is adjusted such that the theoretical and experimental curves coincide at locking ($v_\phi = 0$). Model-required values of τ_M are shown in Fig. 10 for each plasma. With the fit value of τ_M , as well as all the other input parameters, the model is used to generate the time-dependent mode velocity over the entire period of deceleration. The model-calculated mode velocity is then combined with the measured mode amplitude to produce each theoretical braking curve.

The theoretical curves in Fig. 10 are a good match to the experimental curves. As implied above, this is *not* a result of simple curve fitting. Each model curve could, in principle, deviate substantially from the experimental curves. This is one indication that the model is performing well in these plasmas—i.e., that the mode braking is well described by this model. The proximity of τ_M to experimental values is the other criterion by which we gauge the model's success. We show in the next subsection that the model-required val-

TABLE II. For three ensembles of different plasma type, number of shots in the ensemble, plasma fuel, toroidal magnetic field reversal parameter, toroidal plasma current, central line-averaged electron density, normalized growth rate of the QSH mode, normalized mode amplitude at which locking occurs, and the modeled momentum confinement time. All data after the first three rows are ensemble averaged. The reversal parameter is held constant in each case.

	Case I	Case II	Case III
Number of shots	6	8	4
Fuel isotope	H ₂	D ₂	D ₂
F	0.0	0.0	-0.2
I_ϕ (kA)	265±23	284±14	384±7
$\langle n_e \rangle$ (10 ¹⁹ m ⁻³)	1.2±0.3	0.9±0.1	1.0±0.1
Growth rate (%/ms)	0.8±0.2	0.6±0.1	0.3±0.1
$b_\theta/B(a)$ at locking (%)	3.3±0.3	3.2±0.3	1.9±0.2
τ_M (ms)	1.3±0.3	1.9±0.4	2.1±0.1

ues of τ_M are quite consistent with what has been measured experimentally.

F. Comparison of modeled and experimental momentum confinement times

In Table II is a summary of experimental and model data from all the plasmas included in this study. The data shown in Fig. 10 are from the three cases in Table II. The plasmas are grouped by fuel isotope and toroidal field reversal parameter. Although there are important parametric differences between the three cases, the shot-averaged model predictions for τ_M , shown in the bottom row, are all of the order of 1–2 ms. Furthermore, as reflected by the standard deviations of the values of τ_M , the shot-to-shot variation in the modeled τ_M within each ensemble is not large. Slightly later in this section, we shall compare these model predictions to what is measured and expected experimentally.

The modeled value of τ_M is well constrained (precisely determined) in each plasma. We demonstrate this in Fig. 11 by taking the experimental braking curve from Fig. 10(a) and varying τ_M to produce various theoretical braking curves.

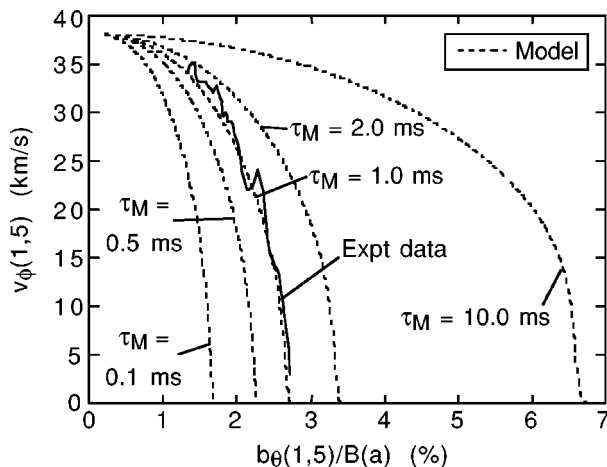


FIG. 11. For the equilibrium and experimental braking curve from the plasma in Fig. 10(a), various modeled braking curves based on different assumed momentum confinement times. The experimental data and original model curve from Fig. 10(a) are included.

We start with $\tau_M = 1.0$ ms, the best fit to the experimental data, and vary it by factors of 2 and 10 ($\tau_M = 0.1, 0.5, 2.0,$ and 10.0 ms). All other parameters are held constant. Clearly, even a factor-of-2 variation in τ_M causes a substantial disagreement between the experimental and model braking curves.

We have not measured τ_M in the specific plasmas studied in this paper, but based on a measurement made in other MST plasmas and some fairly simple arguments, we conclude that the model predictions for τ_M are quite consistent with experimental expectations. The only direct measurement of momentum confinement in MST was reported in Ref. 35, where the deceleration of the plasma was recorded following acceleration with an insertable biased probe. This experiment was carried out in standard-confinement^{21,34} hydrogen plasmas with $I_\phi = 200$ kA, $F = -0.15$, and $\langle n_e \rangle = 0.8 \times 10^{19}$ m⁻³. Based on the data in that paper, one estimates $\tau_M \cong 1.0 - 1.5$ ms.

Over a broad range of plasma parameters, the energy confinement time in MST standard-confinement plasmas falls in the narrow range of about 1.0–2.0 ms.^{21,34} Hence, $\tau_M \sim \tau_E$ in the plasmas studied in Ref. 35. Given the small variation in τ_E in standard MST plasmas, it is reasonable to assume that variations in τ_M will also be fairly small. Such a relation between τ_E and τ_M is observed in tokamaks, where measurements of both quantities are more extensive.³⁶ Hence, we conclude that the values of τ_M shown in Table II are all consistent with experimental values.

One other point of comparison adds to our confidence in the modeling. Compare the predicted values of τ_M in cases I and II in Table II. The primary difference in the background plasma in these two cases is the fuel isotope. The fact that τ_M is predicted to be larger with deuterium is consistent with experimental expectation. The neutral density in the MST plasma core is relatively large, $>0.1\%$ of the electron density,³⁷ and charge exchange of plasma ions with these neutral particles is a significant source of momentum loss. Recent measurements indicate that the central neutral density is smaller in deuterium plasmas than in hydrogen plasmas.³⁸ Thus, τ_M is expected to be larger in deuterium plasmas, consistent with the model prediction.

G. Impact of time-dependent mode growth

To describe the impact of the time-dependent mode growth on the mode braking (i.e., the importance of time dependence in the model), we compare in Fig. 12 four braking curves associated with four different mode growth rates, all linear versus time. The modeled growth rates are variations of that measured in the plasma used in Fig. 10(a). Holding constant the modeled value of τ_M (1.0 ms) in that plasma, we varied the mode growth rate to gauge the predicted impact on the braking curve. The rightmost curve in Fig. 10 corresponds to the experimentally measured growth rate. This is the same as the model curve shown in Fig. 10(a). Working from right to left, the three remaining curves correspond to mode growth rates that are factors of 10, 100, and 1000 times smaller than the original, experimental rate.

There are two important differences between these four

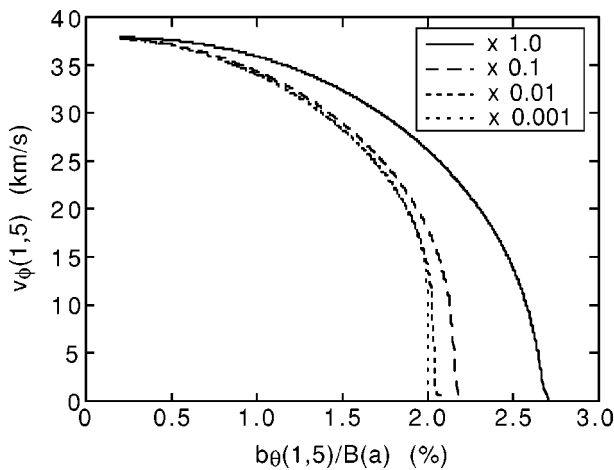


FIG. 12. For the plasma equilibrium and modeled momentum confinement time (1 ms) for the plasma in Fig. 10(a), model-predicted braking curves assuming different mode growth rates, starting with the experimental growth rate ($\times 1.0$) and dividing by successive powers of 10, working from right to left.

curves. One difference is in the value of the mode amplitude at which locking is predicted. The slowest growth rate corresponds to the smallest mode amplitude at locking. The other difference lies in the shape of the curves. In the slowest-growth curve, one can discern an almost discontinuous drop to zero velocity when the velocity reaches $<1/3$ of its initial value. This is similar to what was shown in Fig. 9 for the time-independent model, thus verifying the behavior of the time-dependent model in the limit of very slow mode growth. In contrast to the slowest-growth case, the fastest-growth (experimental) case exhibits no discontinuity. The mode velocity decreases smoothly to zero. This is, of course, what is observed experimentally.

Both of these differences in the predicted braking curves can be explained by comparison of the time scales for mode growth and momentum diffusion. The momentum diffusion time scale $\sim \tau_M = 1.0$ ms, and this is the lower bound on the time scale for the mode to decelerate. The fastest-mode-growth time scale $\tau_{growth} = [(1/b_\theta)(db_\theta/dt)]^{-1} = 1.5$ ms. For the slowest-growing mode, $\tau_{growth} = 1500$ ms.

Consider first the deceleration of the slowest growing mode. Like the time-independent case described earlier, the braking curve for this case can be approximated as a series of torque-balanced equilibria. As the mode amplitude increases, the mode and plasma have a long time, relative to τ_M , to adjust such that the braking and viscous torques come into balance. Eventually, the braking torque becomes large enough that the viscous torque can no longer sustain rotation, and a transition to very slow rotation occurs on a time scale τ_M . During this relatively fast transition in velocity, the slowly growing mode amplitude changes very little, resulting in an approximate vertical discontinuity in the braking curve.

Now consider the fastest-growing mode. There is also a transition point in this case, where the braking torque overpowers the viscous torque, but the deceleration to very slow rotation occurs on the same τ_M time scale. So while this transition is occurring, the mode amplitude has significant time to grow further. This results in the smooth (not discon-

tinuous) drop to very low velocity in the braking curve and accounts for the fact that the mode amplitude at locking is larger than in the slowly growing case.

H. Mode locking

While eddy currents in the shell can significantly retard the QSH dominant mode's rotation, they are unable to actually cause locking. The reason is that, again, the braking torque from the eddy currents approaches zero as the mode velocity approaches zero. Experimentally, however, in all plasmas in which the dominant mode amplitude remains large throughout the deceleration, all of the dominant $m = 1$ modes lock (to within the noise level of the mode velocity measurement). This locking can occur due, e.g., to the finite resonant error field. When the mode velocity is near zero, very little braking torque is required to slow the plasma to the point where the mode rotation is halted completely. In the time-dependent modeling described in this paper, the final asymptotic mode velocity is predicted to be quite small, about 100 000 times smaller than the initial velocity. Hence, locking due to an error field would not be surprising.

VI. SUMMARY AND DISCUSSION

We have described here a fully quantitative, dynamical test of a theory-based model of tearing mode braking due to eddy currents induced in a conducting shell. The model was applied to braking data from MST plasmas with different fuel isotopes, magnetic equilibria, initial mode rotation velocities, and mode growth rates. The global momentum confinement time is the single adjustable parameter in the model and was adjusted such that the theoretical and experimental braking curves in each plasma coincide at locking. That the theoretical curves overlay the experimental curves quite well is one indication that the model works well for these experimental data. Another indication is the good agreement between the model-required and experimental global momentum confinement times.

Consistent with the assumption of viscous coupling between the island plasma and bulk plasma, we have shown that the bulk plasma and the single large mode decelerate on the same time scale. We have also shown that, not surprisingly, the other core-resonant tearing modes also decelerate on this time scale. We have thus shown clear examples of braking due to eddy currents, and in the process, we have also determined the primary cause of the mode deceleration in MST QSH plasmas. This claim is strengthened by the fact that we have ruled out in these plasmas the influence of other, previously established, causes of mode deceleration and locking in MST.

The work described in this paper has several implications for the RFP. First, it bolsters confidence that the time-independent theory published earlier⁹ and the time-dependent extension described here are useful in describing mode deceleration and locking under certain circumstances. Publication of the time-independent theory was motivated primarily by the almost complete lack of mode rotation in the RFX RFP. However, given the lack of mode rotation, comparison between theory and experiment was problematic.

The natural (initial) mode rotation velocity (in the absence of braking torques) had to be estimated based in part on rotation rates in MST, and it was not possible to observe dynamic mode deceleration. The result in the present paper, particularly with the correction to the time-independent braking curve described for RFX, supports the deduction in the earlier paper that eddy currents play a dominant role in preventing mode rotation in that device. The work in this paper also bolsters confidence in the recent modeling³⁹ of the eddy-current braking torque in the rebuilt RFX and the recently commissioned T2R⁴⁰ RFP devices.

QSH plasmas in which a single mode grows to and remains at large amplitude are viewed as possible precursors to as yet *theoretical* plasmas in which the dominant mode grows larger still, and the core-resonant $m=1$ mode spectrum is comprised of only one mode.⁴¹ Such single-helicity plasmas could provide another avenue for substantially improved RFP fusion performance. However, even without modeling, it is clear that the potential for mode braking and locking will be an issue for these plasmas. Techniques to impart momentum to the plasma, such as toroidal neutral beam injection or a rotating external magnetic perturbation, may be needed to maintain plasma rotation. The latter technique was already successfully applied in RFX.⁴²

It is also worth mentioning one other observation regarding modeling of RFP mode rotation in the presence of eddy currents.^{9,39,43} This modeling has been done assuming only one resonant $m=1$ mode. In resistive-shell devices, in particular, the mode amplitude predicted to drive a substantial braking torque is quite small, with a normalized poloidal fluctuation amplitude $\ll 1\%$. It is not uncommon in any RFP for the typically broad spectrum of core-resonant $m=1$ modes to reach this amplitude. This means that substantial braking torque due to eddy currents could be exerted at multiple resonant surfaces in these devices, making deceleration and locking due to eddy currents all the more probable.

This work also has implications for the tokamak. While it certainly does not further prove or disprove the importance of eddy currents in the tokamak, it does show that braking due to eddy currents is possible, and it bolsters confidence in the general model. This work also highlights the importance of the bulk plasma's viscous response, which was not included in early models for the tokamak or RFP.

ACKNOWLEDGMENTS

The authors are grateful to J. S. Sarff for use of his finite-pressure equilibrium reconstruction code and to the MST team for reliable operation of MST. This work was supported by the U.S. DOE.

¹J. A. Snipes, D. J. Campbell, P. S. Haynes *et al.*, Nucl. Fusion **28**, 1085 (1988).

²H. Zohm, A. Kallenbach, H. Bruhns, G. Fussmann, and O. Kluber, Europhys. Lett. **11**, 745 (1990).

³P. R. Brunzell, Y. Yagi, Y. Hirano, Y. Maejima, and T. Shimada, Phys. Fluids B **5**, 885 (1993).

⁴M. F. F. Nave and J. A. Wesson, in *Proceedings of Invited Papers, 14th Conference of the European Physical Society, Madrid, 1987* (European Physical Society, 1987), Vol. 11D, Pt. III, p. 1103.

⁵T. C. Hender, C. G. Gimblett, and D. C. Robinson, in *Proceedings of Invited Papers, 15th Conference of the European Physical Society, Dubrovnik, 1988* (European Physical Society, 1988), Vol. 12B, Pt. I, p. 437.

⁶T. C. Hender, C. G. Gimblett, and D. C. Robinson, Nucl. Fusion **29**, 1279 (1989).

⁷M. F. F. Nave and J. A. Wesson, Nucl. Fusion **30**, 2575 (1990).

⁸R. Fitzpatrick, Nucl. Fusion **7**, 1049 (1993).

⁹R. Fitzpatrick, S. C. Guo, D. J. Den Hartog, and C. C. Hegna, Phys. Plasmas **6**, 3878 (1999).

¹⁰D. A. Gates and T. C. Hender, Nucl. Fusion **36**, 273 (1996).

¹¹Y. Yagi, H. Koguchi, H. Sakakita, S. Sekine, Y. Maejima, J.-A. B. Nilsson, T. Bolzonella, and P. Zanca, Phys. Plasmas **6**, 3824 (1999).

¹²J.-A. Malmberg, P. R. Brunzell, Y. Yagi, and H. Koguchi, Phys. Plasmas **7**, 4184 (2000).

¹³Y. Yagi, H. Koguchi, H. Sakakita, S. Sekine, P. R. Brunzell, and J.-A. Malmberg, Phys. Plasmas **8**, 1625 (2001).

¹⁴I. H. Hutchinson, Plasma Phys. Controlled Fusion **43**, 145 (2001).

¹⁵R. N. Dexter, D. W. Kerst, T. W. Lovell, S. C. Prager, and J. C. Sprott, Fusion Technol. **19**, 131 (1991).

¹⁶A. F. Almagri, S. Assadi, S. C. Prager, J. S. Sarff, and D. W. Kerst, Phys. Fluids B **4**, 4080 (1992).

¹⁷A. K. Hansen, A. F. Almagri, D. J. Den Hartog, S. C. Prager, and J. S. Sarff, Phys. Plasmas **5**, 2942 (1998).

¹⁸C. C. Hegna, Phys. Plasmas **3**, 4646 (1996).

¹⁹J. S. Sarff and A. F. Almagri (private communication).

²⁰D. J. Den Hartog and R. J. Fonck, Rev. Sci. Instrum. **65**, 3238 (1994).

²¹B. E. Chapman, J. K. Anderson, T. M. Biewer *et al.*, Phys. Rev. Lett. **87**, 205 001 (2001).

²²P. Martin, A. Buffa, S. Cappello *et al.*, Phys. Plasmas **7**, 1984 (2000).

²³D. F. Escande, P. Martin, S. Ortolani *et al.*, Phys. Rev. Lett. **85**, 1662 (2000).

²⁴L. Marrelli, P. Martin, G. Spizzo *et al.*, Phys. Plasmas **9**, 2868 (2002).

²⁵P. Martin, L. Marrelli, G. Spizzo *et al.*, Nucl. Fusion **43**, 1855 (2003).

²⁶D. J. Den Hartog, A. F. Almagri, J. T. Chapman, H. Ji, S. C. Prager, J. S. Sarff, R. J. Fonck, and C. C. Hegna, Phys. Plasmas **2**, 2281 (1995).

²⁷V. Antoni, D. Merlin, S. Ortolani, and R. Paccagnella, Nucl. Fusion **26**, 1711 (1986).

²⁸A. K. Hansen, A. F. Almagri, D. Craig, D. J. Den Hartog, C. C. Hegna, S. C. Prager, and J. S. Sarff, Phys. Rev. Lett. **85**, 3408 (2000).

²⁹A. M. Garofalo, E. Eisner, T. H. Ivers *et al.*, Nucl. Fusion **38**, 1029 (1998).

³⁰W. A. Newcomb, Ann. Phys. (N.Y.) **10**, 232 (1960).

³¹C. R. Sovinec, Ph.D. thesis, University of Wisconsin-Madison, Madison, 1995.

³²H. P. Furth, J. Killeen, and M. N. Rosenbluth, Phys. Fluids **6**, 459 (1963).

³³G. Rostagni, Fusion Eng. Des. **25**, 301 (1995).

³⁴T. M. Biewer, Ph.D. thesis, University of Wisconsin-Madison, Madison, 2002.

³⁵A. F. Almagri, J. T. Chapman, C.-S. Chiang, D. Craig, D. J. Den Hartog, C. C. Hegna, and S. C. Prager, Phys. Plasmas **5**, 3982 (1998).

³⁶ITER Physics Basis Editors *et al.*, Nucl. Fusion **39**, 2175 (1999).

³⁷N. E. Lanier, Ph.D. thesis, University of Wisconsin-Madison, Madison, 1999.

³⁸D. Craig, D. J. Den Hartog, G. Fiksel, V. I. Davydenko, and A. A. Ivanov, Rev. Sci. Instrum. **72**, 1008 (2001).

³⁹S. C. Guo and M. S. Chu, Phys. Plasmas **9**, 4685 (2002).

⁴⁰P. R. Brunzell, H. Bergsaker, M. Ceconello, J. R. Drake, R. M. Gravestijn, A. Hedqvist, and J.-A. Malmberg, Plasma Phys. Controlled Fusion **43**, 1457 (2001).

⁴¹D. F. Escande, S. Cappello, F. D'Angelo, P. Martin, S. Ortolani, and R. Paccagnella, Plasma Phys. Controlled Fusion **42**, B243 (2000).

⁴²R. Bartiromo, T. Bolzonella, A. Buffa, G. Chitarin, S. Martini, A. Masiello, and S. Ortolani, Phys. Rev. Lett. **83**, 1779 (1999).

⁴³S. C. Guo and M. S. Chu, Phys. Plasmas **8**, 3342 (2001).